Analysis of DC-Link Voltage Controls in Three-Phase Four-Wire Hybrid Active Power Filters

Wai-Hei Choi, *Student Member, IEEE*, Chi-Seng Lam, *Student Member, IEEE*, Man-Chung Wong, *Senior Member, IEEE*, and Ying-Duo Han, *Senior Member, IEEE*

***Abstract*—This paper investigates different dc-link voltage control strategies in a three-phase four-wire *LC* coupling hybrid active power filter (*LC*-HAPF) for reactive power compensation. By using direct current (current reference) pulsewidth modulation (PWM) control method, to achieve dc-link voltage self-charging function during *LC*-HAPF start-up process, the dc-link voltage control signal feedback as reactive current component is more effective than the traditional method as an active current component. However, when the *LC*-HAPF is performing dynamic reactive power compensation, this dc-link voltage control scheme will influence the reactive power compensation, and thus, makes the *LC*-HAPF lack of success to carry out dynamic reactive power compensation. In this paper, a novel dc-link voltage control scheme for *LC*-HAPF is proposed so that the dc-link voltage control with start-up self-charging process can be obtained as well as providing dynamic reactive power compensation. Representative simulation and experimental results of the three-phase four-wire center-spilt *LC*-HAPF are presented to verify all deductions, and also show the effectiveness of the proposed dc-link voltage control scheme in dynamic reactive power compensation.**

***Index Terms*—Active power filters (APFs), dc-link voltage control, hybrid active power filters (HAPFs), passive power filters (PPFs), reactive power control.**

I. Introduction

IN this modern society, domestic customers' appliances normally draw large harmonic and reactive current from the system. High harmonic current causes various problems in power systems and consumer products, such as overheating in equipment and transformer, blown capacitor fuses, excessive neutral current, low power factor, etc. [1], [2]. On the other hand, loadings with low power factor draw more reactive current than those with high power factor. The larger the reactive current/power, the larger the system current losses and lower the network stability. Thus, electrical utilities usually charge the industrial and commercial customers a higher electricity cost with a low power factor situation.

To eliminate the harmonic and reactive current problems, application of power filters is one of the most suitable solutions. Since the first installation of passive power filters (PPFs) in the mid 1940s, PPFs have been widely used to suppress harmonic current and compensate reactive power in distribution power systems [3] due to their low-cost, simplicity, and high-efficiency characteristics. However, they have many disadvantages such as low dynamic performance, filtering characteristics easily be affected by small variations of the system parameter values and resonance problems [4]–[11].

Since the concept "active ac power filter" was first developed by Gyugyi in 1976 [3], [9], the research studies of the active power filters (APFs) for current quality compensation have been prospered since then. Although APFs overcome the disadvantages inherent in PPFs, the initial and operational costs are relatively high [4]–[10] due to its high dc-link operating voltage during inductive loading. This results in slowing down their large-scale applications in distribution networks.

Later on, different hybrid APF (HAPF) topologies composed of active and passive parts in series and/or parallel have been proposed, in which the active part is a controllable power electronic converter, and the passive part is formed by *RLC* component. This combination aims to improve the compensation characteristics of PPFs and reduces the voltage and/or current ratings (costs) of the APFs, thus providing a cost-effective solution for compensating reactive and harmonic current problems [4]–[18]. Among HAPF topologies in [4]–[13], a transformerless *LC* coupling HAPF (*LC*-HAPF) has been proposed and applied recently for current quality compensation and damping of harmonic propagation in distribution power system [14]–[16], in which it has less passive components and lower dc-link operating voltage comparing with an APF [14].

In addition, *LC*-HAPF is normally designed to deal with harmonic current rather than reactive power compensation [14]–[17], the inverter part is responsible to compensate harmonic currents only and the passive part provides a fixed amount of reactive power. In practical case, the load-side reactive power consumption usually varies from time to time, and if the loading mainly consists of induction motors such as centralized an air-conditioning system, its reactive power consumption will be much higher than the harmonic power consumption [19]. As a result, it is necessary for the *LC*-HAPF to perform dynamic reactive power compensation together with harmonic current compensation.

Manuscript received January 4, 2012; revised May 4, 2012 and July 23, 2012; accepted August 2, 2012. Date of current version November 22, 2012. Recommended for publication by Associate Editor L. M. Tolbert.

W.-H. Choi, C.-S. Lam, and M.-C. Wong are with the Department of Electrical and Computer Engineering, Faculty of Science and Technology, University of Macau, Macao, China (e-mail: da52706@gmail.com; cslam@umac.mo; c.s.lam@ieee.org; mcwong@umac.mo).

Y.-D. Han is with the Department of Electrical Engineering, Tsinghua University, Beijing, China, and also with the Department of Electrical and Computer Engineering, Faculty of Science and Technology, University of Macau, Macao, China (e-mail: ydhan@umac.mo).

Digital Object Identifier 10.1109/TPEL.2012.2214059

All *LC*-HAPF and other HAPFs discussed in [4]–[18] are based on fixed dc-link voltage reference. For the purpose of reducing switching loss and switching noise, an adaptive dc-link voltage reference control is proposed in [20]. However, the author did not discuss the dc-link voltage control in details and also the inherent influence between the reactive power compensation and dc-link voltage controls. Moreover, this influence has not been discussed.

Due to the limitations among the existing literatures, this paper aims to investigate and explore different dc-link voltage control techniques for the three-phase four-wire *LC*-HAPF while performing dynamic reactive power compensation:

1) By using the traditional dc-link voltage control scheme as an active current component, an extra start-up dc-link precharging control process is necessary [5]–[8].
2) To achieve the start-up dc-link voltage self-charging function, a dc-link voltage control as a reactive current component for the *LC*-HAPF is proposed [21]; however, the *LC*-HAPF with this dc-link voltage control scheme fails to provide dynamic reactive power compensation.
3) A novel dc-link voltage control method is proposed for achieving start-up dc-link self-charging function, dc-link voltage control, and dynamic reactive power compensation. Moreover, the proposed method can be applied for the adaptive dc-link voltage reference control as discussed in [20].

In this paper, the designed coupling *LC* is based on the average value of the loading reactive power consumption, while the designed dc-link voltage level is based on the *LC*-HAPF maximum reactive power compensation range specification. Therefore, even though the reactive power compensating range is small with a low dc-link voltage, the *LC*-HAPF can still provide dynamic reactive power compensation. Thus, its reactive power compensation ability (within its specification) is still effective. Given that most of the loads in the distribution power systems are inductive, the following analysis and discussion will only focus on inductive loads [22].

II. A Transformerless Two-Level Three-Phase Four-Wire Center-Spilt *LC*-HAPF

A. *Circuit Structure of LC-HAPF*

The circuit structure of a transformerless three-phase four-wire center-spilt *LC*-HAPF is shown in Fig. 1, where subscript "x" denotes phases *a, b, c,* and n. v_{sx} is the source voltage, v_x is the load voltage, L_s is the source inductor and normally neglected due to its low value relatively; thus, $v_{sx}{\approx}v_x\cdot i_{sx}, i_{Lx}$, and i_{cx} are the source, load, and compensating current for each phase. C_c and L_c are the coupling part capacitor and inductor for each leg of the converter. $C_{\mathrm{dc}U}$, $C_{\mathrm{dc}L}$, $V_{\mathrm{dc}U}$, and $V_{\mathrm{dc}L}$ are the upper and lower dc-link capacitor and dc-link capacitor voltages, and the dc-link voltage $V_{\mathrm{dc}} = V_{\mathrm{dc}U} + V_{\mathrm{dc}L}$. Since the transformerless two-level three-phase four-wire center-spilt *LC*-HAPF can be treated as three independent single-phase circuits, its single-phase equivalent circuit model is shown in Fig. 2.

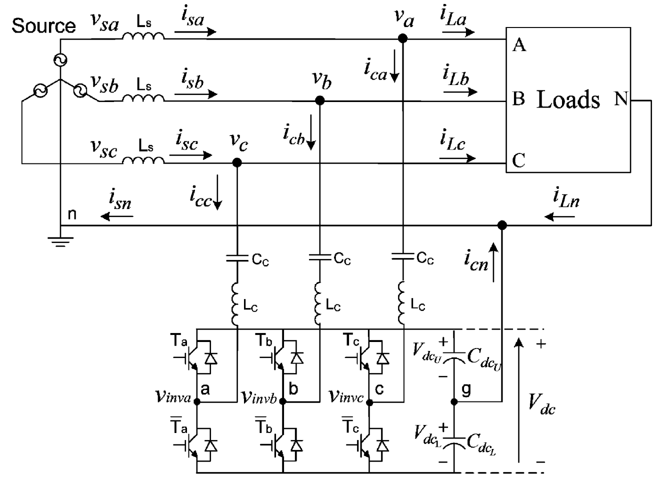

Fig. 1. Circuit structure of a transformerless three-phase four-wire center-spilt *LC*-HAPF.

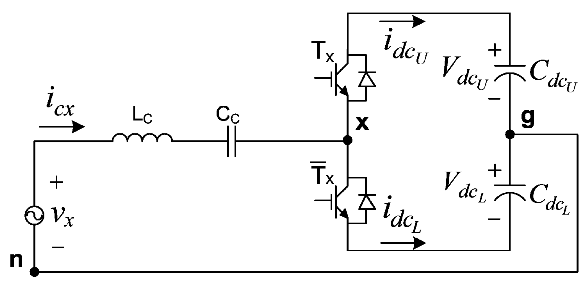

Fig. 2. *S*ingle-phase equivalent circuit model of a three-phase four-wire center-spilt *LC*-HAPF.

B. *Modeling of the DC-Link Voltage in a LC-HAPF Single-Phase Equivalent Circuit*

From Fig. 2, the compensating current i_{cx} can flow either $C_{\mathrm{dc}U}$ or $C_{\mathrm{dc}L}$ and returns through the neutral wire in both directions of insulated-gate bipolar transistors (IGBT) switches. The dc-link capacitor voltages can be expressed as

$$V_{\mathrm{dc}U} = \frac{1}{C_{\mathrm{dc}U}} \int i_{\mathrm{dc}U}\, dt \qquad V_{\mathrm{dc}L} = -\frac{1}{C_{\mathrm{dc}L}} \int i_{\mathrm{dc}L}\, dt \quad (1)$$

where $i_{\mathrm{dc}U}$ and $i_{\mathrm{dc}L}$ are the dc currents of upper and lower dc-link capacitors, respectively, and

$$i_{\mathrm{dc}U} = s_x i_{cx},\; i_{\mathrm{dc}L} = (1 - s_x) i_{cx}. \quad (2)$$

Substituting (2) into (1), the completed upper and lower dc capacitor voltages $V_{\mathrm{dc}U}$ and $V_{\mathrm{dc}L}$ become

$$V_{\mathrm{dc}U} = \frac{1}{C_{\mathrm{dc}U}} \int s_x i_{cx}\, dt$$

$$V_{\mathrm{dc}L} = -\frac{1}{C_{\mathrm{dc}L}} \int i(1 - s_x) i_{cx}\, dt \quad (3)$$

$$s_x = \begin{cases} 1, & \text{if } T_x = 1 \quad \overline{T_x} = 0 \\ 0, & \text{if } T_x = 0 \quad \overline{T_x} = 1. \end{cases} \quad (4)$$

In (3) and (4), s_x represents the switching function of one inverter leg in x phase based on the hysteresis current pulsewidth modulation (PWM) method, and that is the binary state of the

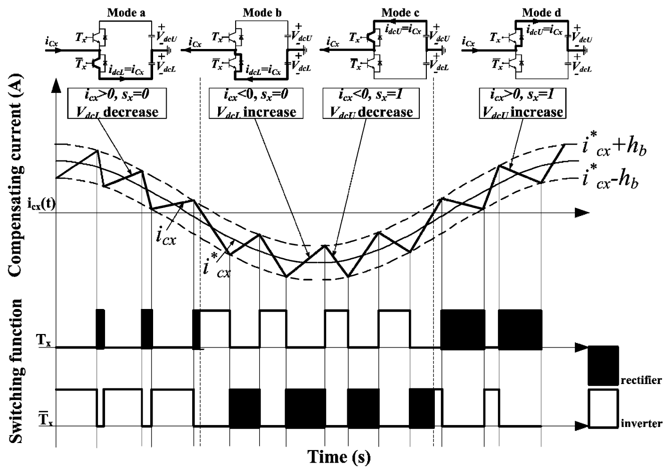

Fig. 3. Operation of a single-phase voltage source inverter under different switching modes by using hysteresis current PWM method.

TABLE I
THE CHANGE OF THE CAPACITOR VOLTAGES ($V_{\mathrm{dc}U}$, $V_{\mathrm{dc}L}$) UNDER DIFFERENT MODES

Switching mode	i_{cx} conditions	Switching function	Operating circuit	Change of dc capacitor voltage
a	$i_{cx}>0$	$s_x=0, T_x=0, \overline{T_x}=1$	Inverter	V_{dcL} decrease
b	$i_{cx}<0$	$s_x=0, T_x=0, \overline{T_x}=1$	Rectifier	V_{dcL} increase
c	$i_{cx}<0$	$s_x=1, T_x=1, \overline{T_x}=0$	Inverter	V_{dcU} decrease
d	$i_{cx}>0$	$s_x=1, T_x=1, \overline{T_x}=0$	Rectifier	V_{dcU} increase

upper and lower switches (T_x and $\overline{T_x}$). When the positive direction of i_{cx} is assumed as Fig. 2, the switching logic for each phase is formulated as [23]: if $i_{cx} > (i^*_{cx} + h_b), T_x$ is ON and $\overline{T_x}$ is OFF, then $s_x = 1$; if $i_{cx} < (i^*_{cx} - h_b), T_x$ is OFF and $\overline{T_x}$ is ON, then $s_x = 0$, where i^*_{cx} is the reference compensating current and h_b is the width of the hysteresis band.

According to the mathematical model in (3), if compensating current $i_{cx} > 0$, the upper dc-link voltage $V_{\mathrm{dc}U}$ is increased during switching function $s_x = 1$, while the lower dc-link voltage $V_{\mathrm{dc}L}$ is decreased for $s_x = 0$. The inverse results can be obtained if $i_{cx} < 0$. Fig. 3 shows the operation of a single-phase voltage source inverter under different switching modes by using hysteresis current PWM method [24]. The changes of the upper and lower dc-link voltages $V_{\mathrm{dc}U}$ and $V_{\mathrm{dc}L}$ under different modes are summarized in Table I.

III. INFLUENCE ON DC-LINK VOLTAGE DURING *LC*-HAPF PERFORMS REACTIVE POWER COMPENSATION

This section aims to present and analyze the influence on the dc-link voltage when *LC*-HAPF performs reactive power compensation. Through this analysis, the dc-link capacitor voltage will either be increased or decreased during fundamental reactive power compensation under insufficient dc-link voltage. Moreover, the influence is proportional to the difference between the *LC*-HAPF compensating current i_{cx} and its pure reactive reference $i^*_{cx_{fq}}$, where the subscript "f," "p," and "q" denote fundamental, active, and reactive components.

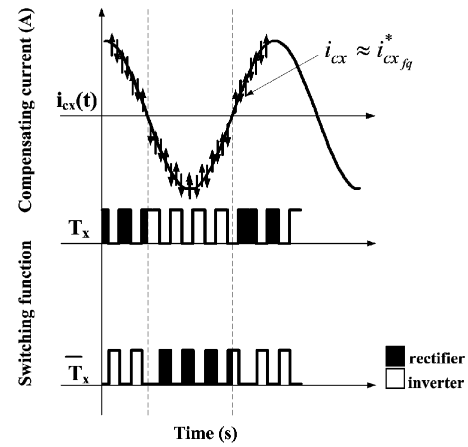

Fig. 4. i_{cx} and $i^*_{cx_{fq}}$ during $I_{cx} \approx I^*_{cx_{fq}}$ case and the corresponding switching function.

A. Reactive Power Compensation Under Sufficient DC-Link Voltage

Under sufficient dc-link voltage, the compensating current generated by the *LC*-HAPF i_{cx} can track its pure reactive reference $i^*_{cx_{fq}}$, as shown in Fig. 4, thus the amplitude $I^*_{cx_{fq}} \approx I_{cx}$. Provided that the hysteresis band is small enough for the *LC*-HAPF to be operated at linear region [25], the PWM switching function in (4) will be evenly distributed, as shown in Fig. 4. According to Table I, the *LC*-HAPF will be changed between the operating modes of rectifier and inverter (modes a, b, c, and d), and keeping the average dc-link voltage as a constant. In ideal lossless case, the dc-link voltage will not be affected when *LC*-HAPF performs reactive power compensation during $I^*_{cx_{fq}} \approx I_{cx}$ case.

B. Reactive Power Compensation Under Insufficient DC-Link Voltage

Under insufficient dc-link voltage, the compensating reactive current generated by the *LC*-HAPF i_{cx} cannot track its pure reactive reference $i^*_{cx_{fq}}$, in which there are two possible situations: 1) If the amplitude $I_{cx} > I^*_{cx_{fq}}$; thus, the instantaneous relationship gives $i_{cx} > i^*_{cx_{fq}}$ during $i_{cx} > 0$, and $i_{cx} < i^*_{cx_{fq}}$ during $i_{cx} < 0$, as shown in Fig. 5; 2) If the amplitude $I_{cx} < I^*_{cx_{fq}}$, the opposite instantaneous relationship is given as shown in Fig. 6.

Hence, to force the compensating current i_{cx} to track its reference $i^*_{cx_{fq}}$ correspondingly:

1) For $I_{cx} > I^*_{cx_{fq}}$ case, as shown in Fig. 5, when the hysteresis band is relatively small compared with the difference between i_{cx} and $i^*_{cx_{fq}}$, their instantaneous relationship between i_{cx} and $i^*_{cx_{fq}}$ can be expressed as follows:

$$i_{cx} > (i^*_{cx_{fq}} + h_b) \qquad \text{for } i_{cx} > 0 \tag{5}$$

$$i_{cx} < (i^*_{cx_{fq}} - h_b) \qquad \text{for } i_{cx} < 0. \tag{6}$$

Based on the hysteresis PWM technique, the switching functions of (5) and (6) are

$$s_x = 1(T_x = 1, \overline{T_x} = 0) \qquad \text{for } i_{cx} > 0 \tag{7}$$

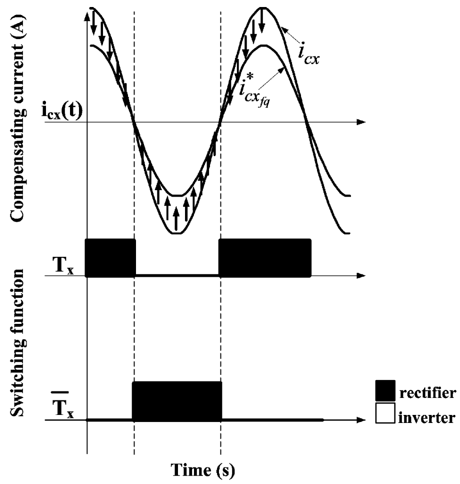

Fig. 5. i_{cx} and $i^*_{cx_{fq}}$ during $I_{cx} > I^*_{cx_{fq}}$ case and the corresponding switching function.

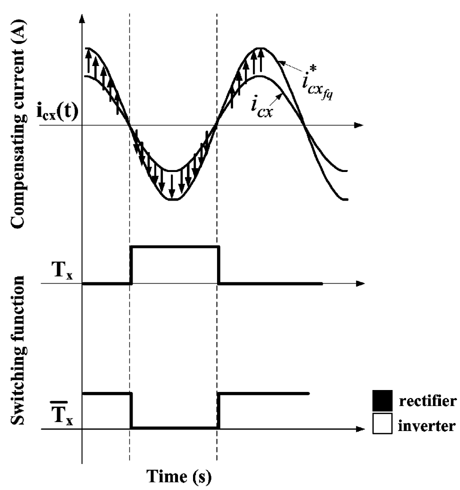

Fig. 6. i_{cx} and $i^*_{cx_{fq}}$ during $I_{cx} < I^*_{cx_{fq}}$ case and the corresponding switching function.

$$s_x = 0(T_x = 0, \overline{T_x} = 1) \qquad \text{for } i_{cx} < 0. \tag{8}$$

According to Table I, the PWM switching sequences in (7) and (8) drive the *LC*-HAPF to be operated in rectifier mode (modes b and d), thus increasing the average dc-link capacitor voltage. When the dc-link voltage is increased to sufficient high level, the *LC*-HAPF will change the operating mode from $I_{cx} > I^*_{cx_{fq}}$ into $I_{cx} \approx I^*_{cx_{fq}}$, and keeping the dc-link voltage value. Therefore, for a given fundamental reactive current reference $i^*_{cx_{fq}}$ $(I_{cx} > I^*_{cx_{fq}})$, the dc-link voltage of *LC*-HAPF will be self-increased to a voltage level that lets the reference compensating current can be tracked.

1) For $I_{cx} < I^*_{cx_{fq}}$ case, as shown in Fig. 6, the instantaneous relationship between i_{cx} and $i^*_{cx_{fq}}$ is

$$i_{cx} < (i^*_{cx_{fq}} + h_b) \qquad \text{for } i_{cx} > 0 \tag{9}$$

$$i_{cx} > (i^*_{cx_{fq}} - h_b) \qquad \text{for } i_{cx} < 0. \tag{10}$$

The switching functions of (9) and (10) are

$$s_x = 0(T_x = 0, \overline{T_x} = 1) \qquad \text{for } i_{cx} > 0 \tag{11}$$

$$s_x = 1(T_x = 1, \overline{T_x} = 0) \qquad \text{for } i_{cx} < 0. \tag{12}$$

According to Table I, the PWM switching sequences in (11) and (12) drive the *LC*-HAPF to be operated in inverter mode (modes a and c), thus decreasing the average dc-link capacitor voltage.

IV. *LC*-HAPF Operation by Conventional DC-Link Voltage Control Methods

A. DC-Link Voltage Control Method as Active Current Component

Traditionally, if the indirect current (voltage reference) PWM control method is applied, the dc-link voltage of the inverter is controlled by the reactive current component feedback signal [5]–[8], [14]–[18]. However, when the direct current PWM control method is applied in [5]–[8], and [14]–[18], the dc-link voltage should be controlled by the active current component feedback signal. Both dc-link voltage control methods are equivalent to each other.

When *LC*-HAPF performs reactive power compensating, the reference compensating current i^*_{cx} is composed by

$$i^*_{cx} = i^*_{cx_{fq}} + i^*_{cx_{fp\_dc}} = i^*_{Lx_{fq}} + i^*_{cx_{fp\_dc}} \tag{13}$$

where $i^*_{cx_{fp\_dc}}$ is the dc-link voltage controlled signal related to active current component, and $i^*_{Lx_{fq}}$ is the loading fundamental reactive current that is equal to the reference compensating fundamental reactive current $i^*_{cx_{fq}}$, $i^*_{cx_{fq}} = i^*_{Lx_{fq}}$.

However, to perform the reactive power and dc-link voltage control action in (13), a sufficient dc-link voltage should be provided to let the compensating current i_{cx} track with its reference i^*_{cx}. As a result, this conventional dc-link voltage control method fails to control the dc-link voltage during insufficient dc-link voltage, such as during start-up process. Due to this reason, when this dc-link voltage control method is applied in *LC*-HAPF, an extra start-up precharging control process is necessary. Usually, a three-phase uncontrollable rectifier is used to supply the initial dc-link voltage before operation [5]–[8]. Moreover, when the adaptive dc-link voltage control idea is applied, the reference dc-link voltage may be changed from a low level to a high level; at that occasion, the dc-link voltage may be insufficient to track the new reference value. Therefore, the conventional dc-link voltage control with precharging method may not work properly in the adaptive dc-link voltage controlled system [20].

The *LC*-HAPF in [14]–[16] showed that this dc-link voltage control can achieve start-up self-charging function without any external supply. That is actually due to the *LC*-HAPF in [14]–[16], which is initially operating at $I_{cx} > I^*_{cx_{fq}}$ condition. According to the analysis in Section III, during $I_{cx} > I^*_{cx_{fq}}$ condition, the dc-link voltage will be self-charging to a sufficient voltage level that lets the *LC*-HAPF's compensating current track with its reference $i^*_{cx_{fq}} \approx i_{cx}$. Thus, the dc-link voltage can be maintained as its reference value in

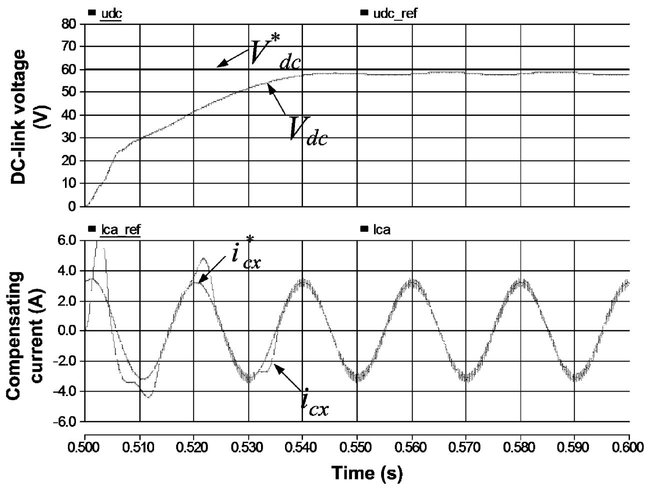

Fig. 7. $V_{\rm dc}, i^*_{cx}$, and i_{cx} during $I_{cx} > I^*_{cx_{fq}}$ condition with conventional dc-link voltage control method as active current component.

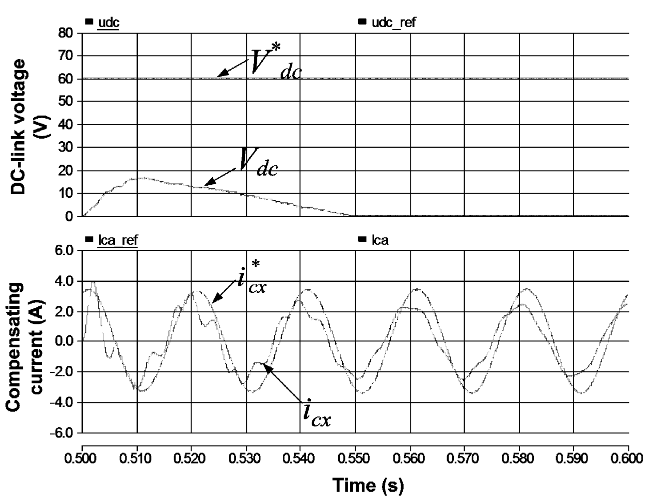

Fig. 8. $V_{\rm dc}, i^*_{cx}$, and i_{cx} during $I_{cx} < I^*_{cx_{fq}}$ condition with conventional dc-link voltage control method as active current component.

steady state. However, if the *LC*-HAPF is initially operating at $I_{cx} < I^*_{cx_{fq}}$ condition, this dc-link voltage control method fails to carry out this function.

Figs. 7 and 8 show the simulation results of *LC*-HAPF start-up process by using the conventional dc-link voltage control method under different cases. From Fig. 7, when *LC*-HAPF starts operation during $I_{cx} > I^*_{cx_{fq}}$ condition, the dc-link voltage $V_{\rm dc}$ can carry out the start-up self-charging function and $i^*_{cx} \approx i_{cx}$ in steady state. On the contrary, from Fig. 8, neither the dc-link voltage nor the reactive power compensation can be controlled when *LC*-HAPF is operating during $I_{cx} < I^*_{cx_{fq}}$ condition, in which the simulation results verified the previous analysis.

B. DC-Link Voltage Control Method as Reactive Current Component

According to the analysis in Section III, the dc-link voltage can be influenced by varying the reference compensating fundamental reactive current $i^*_{cx_{fq}}$ under insufficient dc-link voltage; thus, the dc-link voltage can also be controlled by utilizing this influence. Hence, this dc-link voltage control method can achieve the start-up self-charging function. Moreover, it has been shown that this method is more effective than that conventional method as active current component [21]. However, when it is being applied in *LC*-HAPF, although the dc-link voltage can be controlled as its reference value, the *LC*-HAPF cannot perform dynamic reactive power compensation. The corresponding reason can be derived as follows.

By using the dc-link voltage control method as reactive current component, the reference compensating current i^*_{cx} is composed by

$$i^*_{cx} = i^*_{cx_{fq}} = i^*_{Lx_{fq}} + i^*_{cx_{fq\_{\rm dc}}} \tag{14}$$

where $i^*_{cx_{fq\_{\rm dc}}}$ is the dc-link voltage control signal related to reactive current component.

Based on the analysis in Section III, under insufficient dc-link voltage, the change of the dc-link voltage is directly proportional to the difference between the amplitude of I_{cx} and $I^*_{cx_{fq}}$. Moreover, it has been concluded that for a given reference $i^*_{cx_{fq}}$ ($I_{cx} > I^*_{cx_{fq}}$), the dc-link voltage will be self-charging to a voltage level, then i_{cx} can trend its reference $i^*_{cx_{fq}}$ gradually, and maintaining this voltage level in steady state. Therefore, to control the dc-link voltage $V_{\rm dc}$ as its reference $V^*_{\rm dc}$, it will have a corresponding fixed reference value, that is, $I^*_{cx_{fq}} = I^*_{cx_{fq\_{\rm fixed}}}$. Therefore

$$V^*_{\rm dc}|_{I^*_{cx_{fq}} = I^*_{cx_{fq\_{\rm fixed}}}} - V_{\rm dc} = 0. \tag{15}$$

Equation (15) implies that to control the dc-link voltage, the *LC*-HAPF must restrict to provide a fixed amount of reactive power. Therefore, by using the dc-link voltage control method as reactive current component, the *LC*-HAPF fails to perform dynamic reactive power compensation, in which the corresponding simulation and experimental results will be given in Section VI.

V. Proposed DC-Link Voltage Control Method

From the previous analysis, the dc-link voltage control method as active current component is effective only under sufficient dc-link voltage. In an insufficient dc-link voltage case, such as the *LC*-HAPF start-up process, both dc-link voltage control and reactive power compensation may fail. On the contrary, when the dc-link voltage control method as reactive current component is applied, the dc-link voltage control can be effectively controlled with start-up self-charging function. However, by using this control method, the *LC*-HAPF fails to perform dynamic reactive power compensation. As a result, a novel dc-link voltage control method by both reactive and active current components as the feedback signals is proposed in this section, so as to combine the advantages of both methods, which can achieve the start-up self-charging function, dc-link voltage control, and dynamic reactive power compensation.

$$\Delta Q_{\rm dc} = -k_q \cdot (V^*_{\rm dc} - V_{\rm dc}) \tag{16}$$

$$\Delta P_{\rm dc} = k_p \cdot (V^*_{\rm dc} - V_{\rm dc}) \tag{17}$$

where $\Delta Q_{\rm dc}$ and $\Delta P_{\rm dc}$ are the dc control signals related to the reactive and active current components and k_q and k_p are the corresponding positive gains of the controller. By using the proposed control method, the reference compensating current i^*_{cx} is calculated by

$$i^*_{cx} = i^*_{cx_{fq}} + i^*_{cx_{fp\_{\rm dc}}} \tag{18}$$

where $i^*_{cx_{fq}} = i^*_{Lx_{fq}} + i^*_{cx_{fq\_{\rm dc}}}$.

In (17), $\Delta P_{\rm dc}$ represents the active power flow between the source and the LC-HAPF compensator, $\Delta P_{\rm dc} > 0$ means the *LC*-HAPF absorbs active power from the source, and $\Delta P_{\rm dc} < 0$ means the *LC*-HAPF injects active power to the source [26]. According to the analysis in Section III, the dc-link voltage will be charged for $I_{cx} > I^*_{cx_{fq}}$, and discharged for $I_{cx} < I^*_{cx_{fq}}$ during performing reactive power compensation. When $V^*_{\rm dc} - V_{\rm dc} > 0$, in order to increase the dc-link voltage, $I^*_{cx_{fq}}$ should be decreased by adding a negative $\Delta Q_{\rm dc}$. On the contrary, when $V^*_{\rm dc} - V_{\rm dc} < 0$, in order to decrease the dc-link voltage, $I^*_{cx_{fq}}$ should be increased by adding a positive $\Delta Q_{\rm dc}$. Therefore, the "$-$" sign is added in (16). In this paper, in order to simplify the control process, $\Delta Q_{\rm dc}$ and $\Delta P_{\rm dc}$ in (16) and (17) are calculated by the same controller, i.e., $k_q = k_p$.

In (18), $i^*_{Lx_{fq}}$, $i^*_{cx_{fq\_{\rm dc}}}$, and $i^*_{cx_{fp\_{\rm dc}}}$ are calculated by using the three-phase instantaneous $p-q$ theory [27]

$$\begin{bmatrix} i^*_{La_{fq}} \\ i^*_{Lb_{fq}} \\ i^*_{Lc_{fq}} \end{bmatrix} = \sqrt{\frac{2}{3}} \times \frac{1}{v_0 v^2_{\alpha\beta}} \begin{bmatrix} 1/\sqrt{2} & 1 & 0 \\ 1/\sqrt{2} & -1/2 & \sqrt{3}/2 \\ 1/\sqrt{2} & -1/2 & -\sqrt{3}/2 \end{bmatrix} \times \begin{bmatrix} v^2_{\alpha\beta} & 0 & 0 \\ 0 & v_0 v_\alpha & -v_0 v_\beta \\ 0 & v_0 v_\beta & v_0 v_\alpha \end{bmatrix} \begin{bmatrix} 0 \\ 0 \\ q_{\alpha\beta} \end{bmatrix} \tag{19}$$

$$\begin{bmatrix} i^*_{ca_{fq\_{\rm dc}}} \\ i^*_{cb_{fq\_{\rm dc}}} \\ i^*_{cc_{fq\_{\rm dc}}} \end{bmatrix} = \sqrt{\frac{2}{3}} \times \frac{1}{v_0 v^2_{\alpha\beta}} \begin{bmatrix} 1/\sqrt{2} & 1 & 0 \\ 1/\sqrt{2} & -1/2 & \sqrt{3}/2 \\ 1/\sqrt{2} & -1/2 & -\sqrt{3}/2 \end{bmatrix} \times \begin{bmatrix} v^2_{\alpha\beta} & 0 & 0 \\ 0 & v_0 v_\alpha & -v_0 v_\beta \\ 0 & v_0 v_\beta & v_0 v_\alpha \end{bmatrix} \begin{bmatrix} 0 \\ 0 \\ \Delta Q_{\rm dc} \end{bmatrix} \tag{20}$$

$$\begin{bmatrix} i^*_{ca_{fp\_{\rm dc}}} \\ i^*_{cb_{fp\_{\rm dc}}} \\ i^*_{cc_{fp\_{\rm dc}}} \end{bmatrix} = \sqrt{\frac{2}{3}} \times \frac{1}{v_0 v^2_{\alpha\beta}} \begin{bmatrix} 1/\sqrt{2} & 1 & 0 \\ 1/\sqrt{2} & -1/2 & \sqrt{3}/2 \\ 1/\sqrt{2} & -1/2 & -\sqrt{3}/2 \end{bmatrix} \times \begin{bmatrix} v^2_{\alpha\beta} & 0 & 0 \\ 0 & v_0 v_\alpha & -v_0 v_\beta \\ 0 & v_0 v_\beta & v_0 v_\alpha \end{bmatrix} \begin{bmatrix} 0 \\ \Delta P_{\rm dc} \\ 0 \end{bmatrix} \tag{21}$$

where $q_{\alpha\beta}$ are the three-phase loading reactive power consumption, v_α, v_β, and v_0 are the load voltages on the $\alpha-\beta-0$ coordinate after the Clarke transformation [27], and $v_{\alpha\beta} = v^2_\alpha + v^2_\beta$.

Fig. 9 shows the control process of the proposed dc-link voltage control method, when the *LC*-HAPF starts operation, the dc-link voltage is insufficient to let the compensating current i_{cx} track with its reference i^*_{cx}. Thus, the dc-link voltage control signal as reactive current component will dominate the control action in (18). During this period, the dc-link voltage will be self-charging under $I_{cx} > I^*_{cx_{fq}}$ condition. As the dc-link voltage is increased and approaching the reference value, the compensating current tracking ability of the *LC*-HAPF will be improved gradually, and the control signals $\Delta Q_{\rm dc}$ and $\Delta P_{\rm dc}$ in (16) and (17) will also be decreased gradually; thus, $i^*_{cx} \approx i_{cx}$ eventually. According to the analysis in Section III, the dc-link voltage will not be affected by the reactive component when $i^*_{cx} \approx i_{cx}$. Hence, during this period, the dc-link voltage control signal as active current component will dominate the control action in (18). Therefore, the proposed dc-link voltage control method can be realized as:

1) $\Delta Q_{\rm dc}$ control signal is used to step change the dc-link voltage under insufficient dc-link voltage that can be effectively applied for start-up process and the adaptive dc-link voltage control [20];
2) $\Delta P_{\rm dc}$ control signal is used to maintain the dc-link voltage under sufficient dc-link voltage.

By using the proposed method, the *LC*-HAPF can compensate the reactive power consumed by the load, and keep the dc-link voltage as its reference one as shown in Fig. 9 ($Q_{sx_f} \approx 0$ var, $V_{{\rm dc}U} = V_{{\rm dc}L} = V^*_{\rm dc}/2 = 30$ V). Therefore, the proposed dc-link voltage control method can effectively control the dc-link voltage without any extra precharging process and lets the *LC*-HAPF provide dynamic reactive power compensation. Table II shows the comparison among the conventional and proposed dc-link voltage control methods.

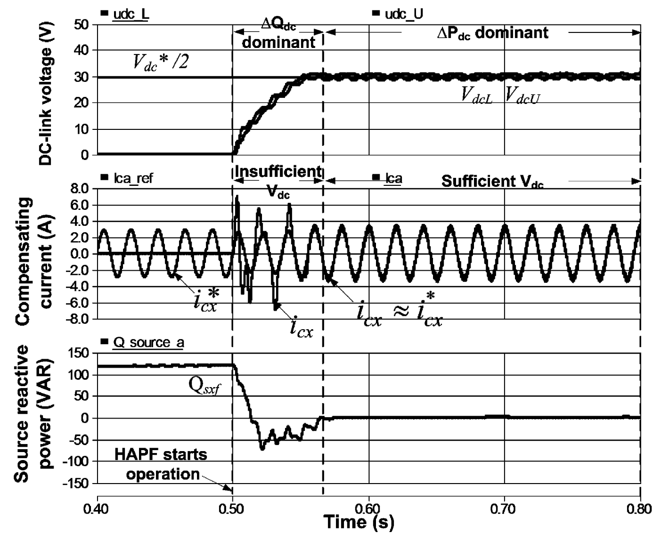

Fig. 9. Control process of the proposed dc-link voltage control method.

TABLE II
COMPARISON BETWEEN CONVENTIONAL AND PROPOSED DC-LINK CONTROL METHODS

Functions	DC-link voltage control methods		
	Feedback as active current component [5] – [8], [14] – [18]	Feedback as reactive current component [21]	Proposed
Start-up self-charging	X	O	O
DC-link voltage control	O*	O	O
Adaptive dc-link voltage control [20]	O*	O	O
Dynamic reactive power compensation	O*	X	O

Note: O – function, X – failure, O* – conditionally can work under sufficient current tracking ability.

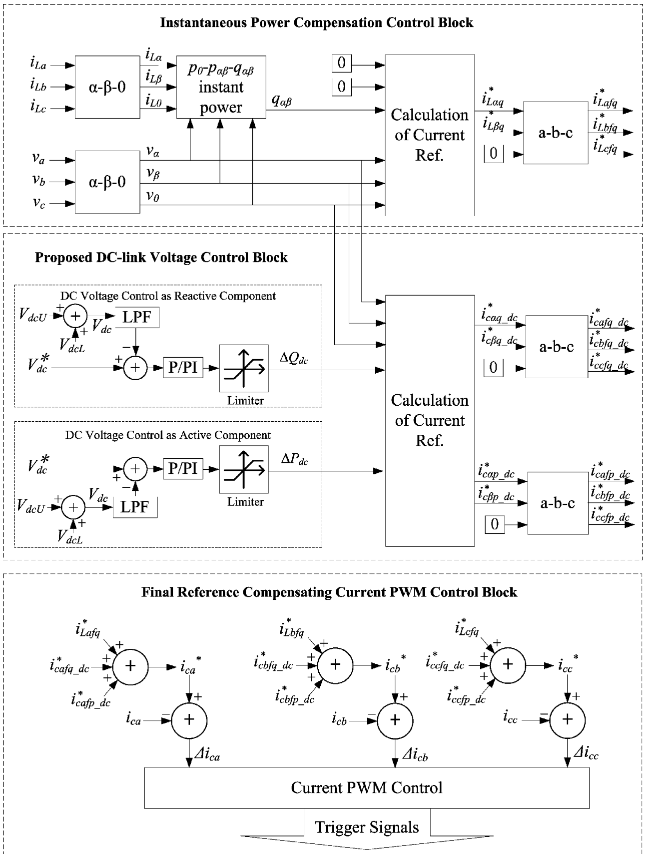

Fig. 10. Control block diagram for the three-phase four-wire *LC*-HAPF by using proposed dc-link voltage control method.

Fig. 10 shows the control block diagram of the proposed dc-link voltage control method of the three-phase four-wire *LC*-HAPF, in which it consists of three main control blocks: 1) instantaneous power compensation control block; 2) proposed dc-link voltage control block; and 3) final reference compensating current PWM control block.

1) For the instantaneous power compensation control block, the loading fundamental reactive currents $i^*_{Lx_{fq}}$ are determined by the three-phase instantaneous $p-q$ theory [27].
2) The dc-link voltage is controlled by the proposed method. The dc-link voltage $V_{\rm dc}$ is first obtained by summing up the measured upper and lower dc-link capacitor voltages ($V_{{\rm dc}U}$ and $V_{{\rm dc}L}$). A low-pass filter (LPF) is applied to filter out high-frequency noise. Then, the signal $V_{\rm dc}$ is compared with the reference value $V^*_{\rm dc}$, and their difference will input to the proportional P controller to obtain the corresponding dc-link voltage control signals $\Delta Q_{\rm dc}$ and $\Delta P_{\rm dc}$. If the proportional gains k_q and k_p in (16) and (17) are set too large, the stability of the control process will be degraded, and produces a large fluctuation during steady state. On the contrary, if proportional gains are set too small, a long settling time and a large steady-state error will occur. Moreover, the dc-link voltage control method can also be applied by PI controller, the integral term can accelerate the movement of the process toward the reference value and eliminate the residual steady-state error. Since the parameter design of the dc-link voltage controller is not the main theme of this paper, a pure proportional controller with an appropriate value is selected. A limiter is applied to avoid the overflow problem. After that, the final dc-link voltage control reference currents $i^*_{cx_{fq\_{\rm dc}}}$ and $i^*_{cx_{fp\_{\rm dc}}}$ can be calculated, and they will be sent to current PWM control block to perform the dc-link voltage control.
3) Then, the final reference compensating current i^*_{cx} can be obtained by summing up the $i^*_{Lx_{fq}}$, $i^*_{cx_{fq\_{\rm dc}}}$, and $i^*_{cx_{fp\_{\rm dc}}}$. Then i^*_{cx} together with compensating current i_{cx} will be sent to the current PWM control part for generating PWM trigger signals to control the power electronic switches of the inverter.

TABLE III
LC-HAPF SYSTEM PARAMETERS FOR SIMULATIONS AND EXPERIMENTS

System parameters		Physical values
Source	V_x	$55V_{rms}$
	L_S	1mH
LC-HAPF: (Reactive power supplied by passive part $Q_{cx_f\_PPF} = -145.1VAR$)	L_C, C_C	6mH, 140uF
	$V_{dc}^*/2$	30V
1st inductive loading: $Q_{Lx_f} = 121.8VAR$	R_{L1}, L_{L1}	12Ω, 30mH
1st and 2nd inductive loadings: $Q_{Lx_f} = 176.6VAR$	R_{L1}, L_{L1}	12Ω, 30mH
	R_{L2}, L_{L2}	17.5Ω, 30mH

VI. Simulation and Experimental Verifications

To verify: 1) Failure dynamic reactive power compensation with dc-link voltage control as reactive current component; and 2) effectiveness of the proposed dc-link control method. The simulated and experimental results in a small rating three-phase four-wire center-split *LC*-HAPF under balanced linear inductive loading will be given. Table III lists the simulated and experimental system parameters for the *LC*-HAPF, as shown in Fig. 1. The coupling *LC* is designed based on: 1) an approximate mean value of the reactive power consumption for the first loading and both first and second loadings, and 2) the switching frequency with switching ripple less than 0.5 A with a maximum dc-link voltage of $V^*_{\rm dc}/2 = 40$ V. When the harmonic currents compensation is also taken in consideration, the resonant frequency of the coupling *LC* should also be considered. Moreover, the dc-link voltage reference $V^*_{\rm dc}/2 = 30$ V in Table III is designed based on the minimum dc-link voltage requirement [20]. Simulation studies were carried out by using PSCAD/EMTDC. All control algorithms mentioned in this paper are adopted in the *LC*-HAPF hardware prototype and implemented by a digital signal processor (DSP—TMSS320F2407).

Fig. 11 shows the simulated and experimental reactive power at load side Q_{Lx_f}. When the first inductive loading is connected, the simulated Q_{Lx_f} for three-phase is 121.8 var with displacement power factor (DPF) = 0.786, while the three-phase experimental Q_{Lx_f} are 116.0, 114.5, and 117.8 var with DPF = 0.804, 0.815, and 0.812, respectively. When both the first and second inductive loadings are connected, the simulated Q_{Lx_f} for three-phase increases to 176.6 var with DPF = 0.833, while the

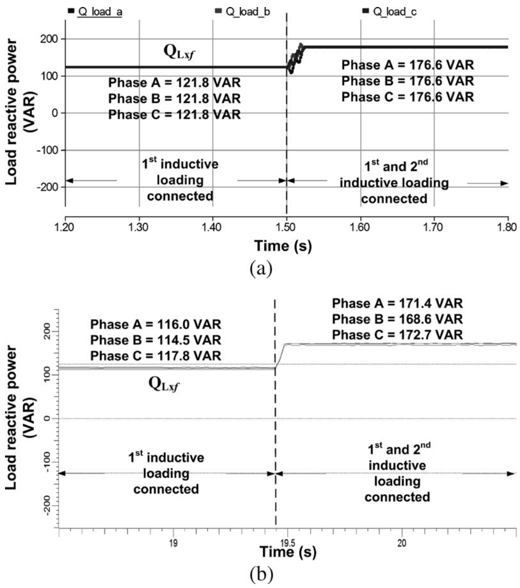

Fig. 11. Load-side fundamental reactive power: (a) simulated Q_{Lxf} and (b) experimental Q_{Lxf}.

TABLE IV

SIMULATION RESULTS BEFORE AND AFTER *LC*-HAPF REACTIVE POWER COMPENSATION WITH DC-LINK VOLTAGE CONTROL METHOD WITH REACTIVE CURRENT COMPONENT

Before Compensation				After Compensation			
Different Cases:	Q_{Lx_f} (VAR)	DPF	i_{sx} (A_{rms})	Q_{sx_f} (VAR)	DPF	i_{sx} (A_{rms})	$THD_{i_{sx}}$ (%)
1st inductive loading	121.8	0.786	3.60	-18.4	0.991	2.90	1.2
1st and 2nd inductive loading	176.6	0.833	6.03	45.1	0.986	5.10	1.0

TABLE V

EXPERIMENTAL RESULTS BEFORE AND AFTER *LC*-HAPF REACTIVE POWER COMPENSATION WITH DC-LINK VOLTAGE CONTROL METHOD WITH REACTIVE CURRENT COMPONENT

Before Compensation					After Compensation			
Different Cases:		Q_{Lx_f} (VAR)	DPF	i_{sx} (A_{rms})	Q_{sx_f} (VAR)	DPF	i_{sx} (A_{rms})	$THD_{i_{sx}}$ (%)
1st inductive loading	A	116.0	0.804	3.48	-23.5	0.974	2.98	6.9
	B	114.5	0.815	3.58	-30.3	0.972	3.07	6.5
	C	117.8	0.812	3.58	-22.6	0.974	2.90	5.9
1st and 2nd inductive loading	A	171.4	0.835	5.85	45.2	0.977	5.16	3.1
	B	168.6	0.842	5.91	42.1	0.980	5.22	3.5
	C	172.7	0.841	5.90	53.4	0.976	5.05	3.5

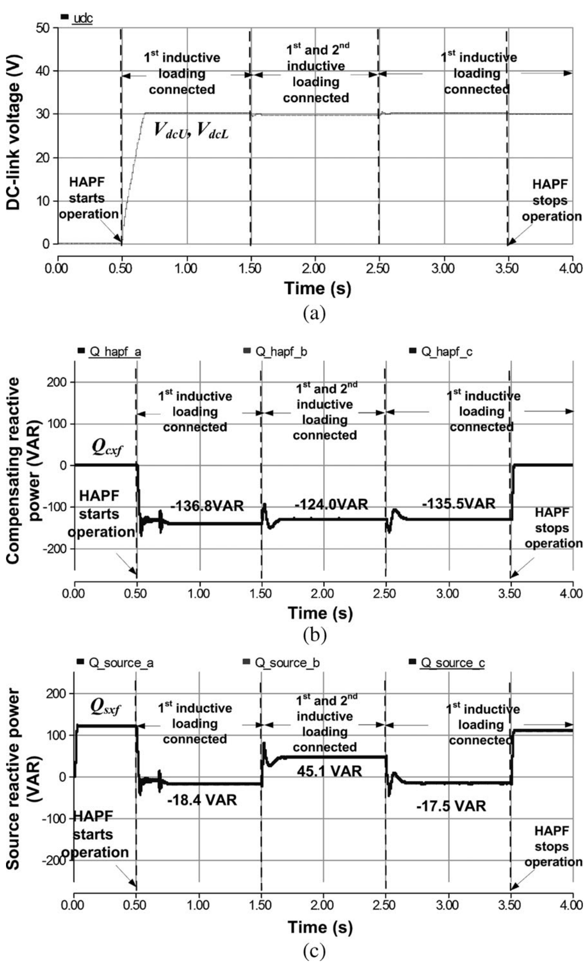

Fig. 12. *LC*-HAPF whole simulated process with dc-link voltage control method with reactive current component: (a) V_{dc_U} and V_{dc_L}, (b) Q_{cxf} of phase a, and (c) Q_{sxf} of phase a.

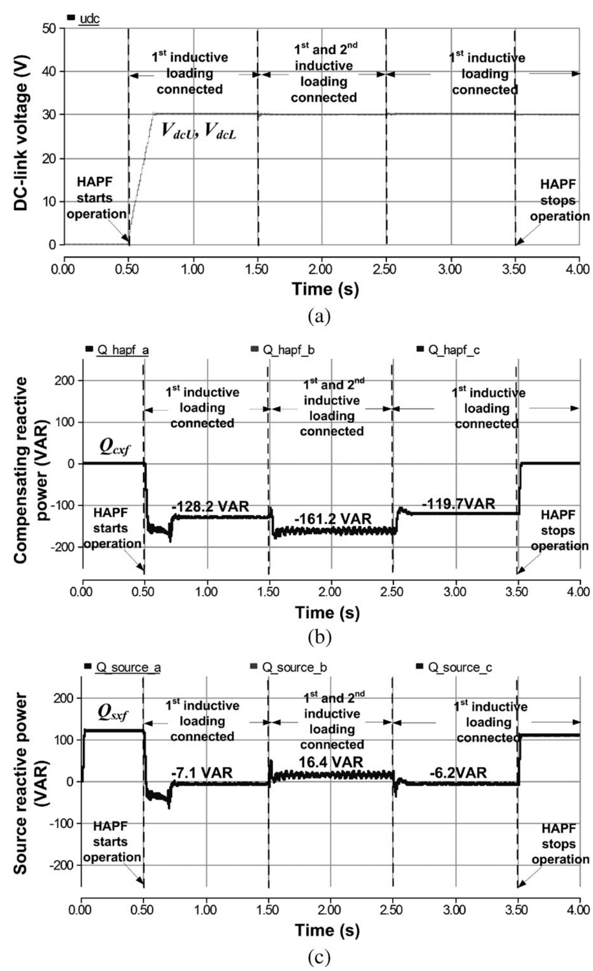

Fig. 13. *LC*-HAPF whole simulated process with proposed dc-link voltage control method: (a) V_{dc_U} and V_{dc_L}, (b) Q_{cxf} of phase a, and (c) Q_{sxf} of phase a.

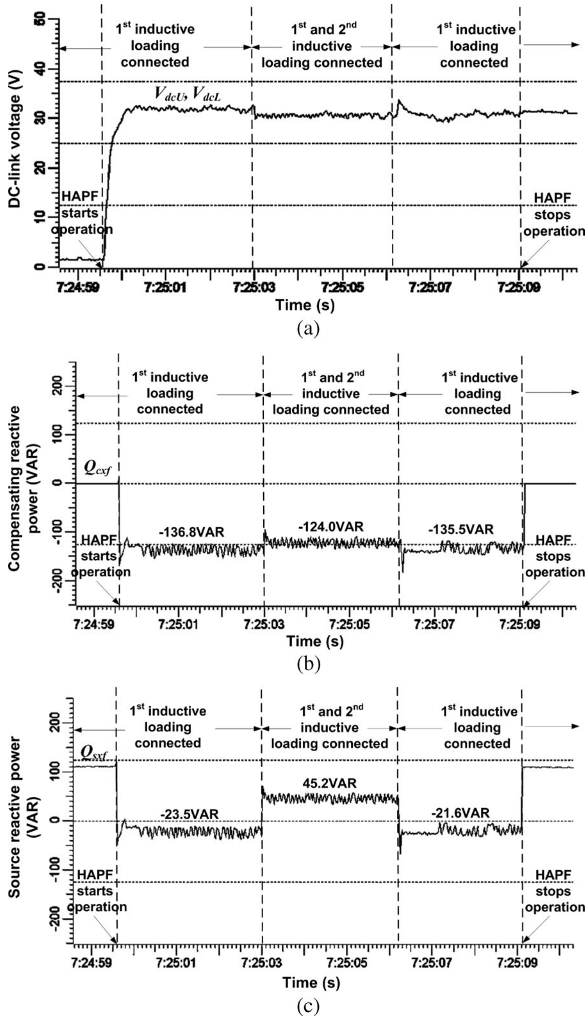

Fig. 14. *LC*-HAPF whole experimental process with dc-link voltage control method with reactive current component: (a) V_{dc_U} and V_{dc_L}, (b) Q_{cxf} of phase a, and (c) Q_{sxf} of phase a.

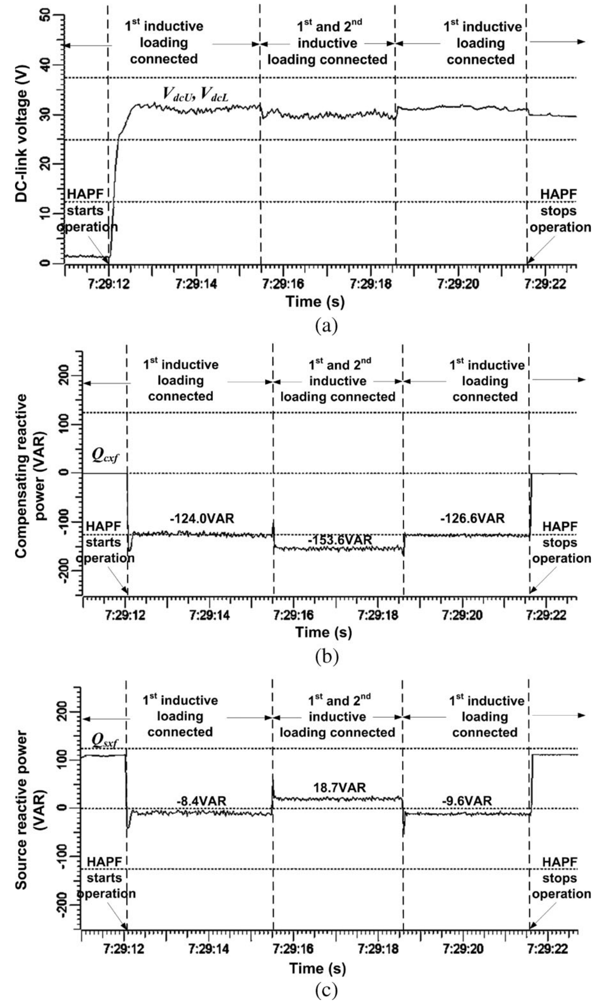

Fig. 15. *LC*-HAPF whole experimental process with proposed dc-link voltage control method: (a) V_{dc_U} and V_{dc_L}, (b) Q_{cxf} of phase a, and (c) Q_{sxf} of phase a.

three-phase experimental Q_{Lx_f} increases to 171.4, 168.6, and 172.7 var with DPF = 0.835, 0.842, and 0.841, respectively.

A. Failure Dynamic Reactive Power Compensation With DC-Link Voltage Control as Reactive Current Component

With the implementation of the dc-link voltage control as reactive current component, Figs. 12 and 14 illustrate the whole simulated and experimental dynamic reactive power compensation process for the loading situations, as shown in Fig. 11, they include the waveforms of: 1) V_{dc_U} and V_{dc_L}, 2) Q_{cx_f} of phase a; and 3) Q_{sx_f} of phase a. Figs. 12(a) and 14(a) show that the simulation and experimental V_{dc_U} and V_{dc_L} level can be controlled as the reference value without any precharging process, and being kept at its reference 30 V no matter when the first inductive loading or first and second loadings are connected, this verifies the effectiveness of the dc-link voltage control as reactive current component. Since the simulated and experimental loadings are approximately balanced, only phase a compensation diagrams will be illustrated. Even though the dc-link voltage can be controlled by this method, Figs. 12(b) and 14(b) illustrate that the simulated and experimental fundamental compensating reactive power Q_{cx_f} are approximately fixed, no matter when the first or first and second loadings are connected. That means the *LC*-HAPF fails to provide dynamic reactive power compensation by using this dc-link voltage control method. This result verifies the previous analysis in Section IV. As a result, the residual reactive power shown in Figs. 12(c) and 14(c) will be supplied by the source side with simulated and experimental Q_{sx_f} of phase $a \approx -18.4$, 45.1 and -23.5, 45.2 var, respectively, when the first inductive loading or first and second loadings are connected.

Tables IV and V summarize the dynamic reactive power compensation results of the *LC*-HAPF based on the dc-link voltage control method with reactive current component. The three-phase simulated and experimental DPF of source-side can be improved when the first loading (or both the first and second loadings) is connected. The simulated and experimental $\mathrm{THD}_{i_{sx}}$ are within 2.0% and 7.0%. Figs. 12 and 14 and Tables IV and V verify the previous analysis of the *LC*-HAPF failure in dynamic reactive power compensation by using conventional dc-link voltage control method as reactive current component.

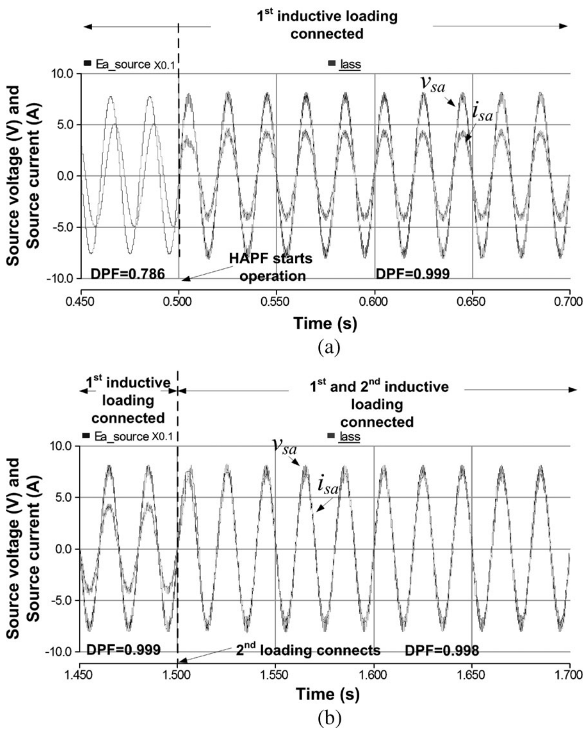

Fig. 16. Simulated dynamic response of *LC*-HAPF by using proposed dc-link voltage control method when (a) the first loading is connected and (b) both the first and second loadings are connected.

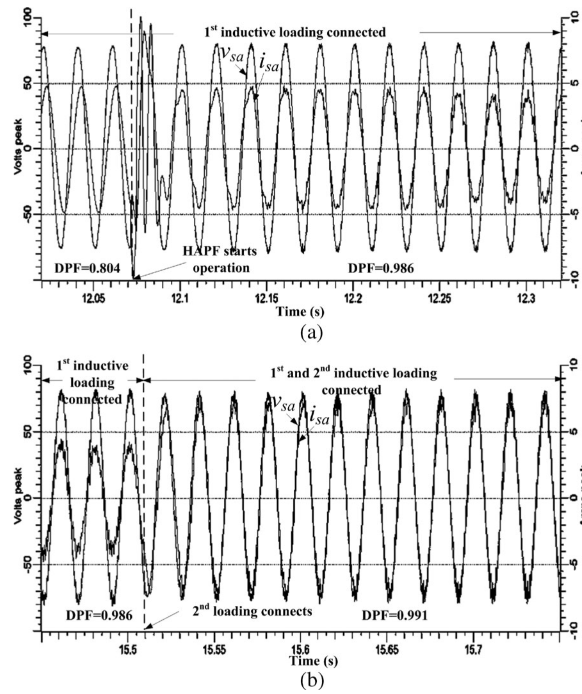

Fig. 17. Experimental dynamic response of *LC*-HAPF by using proposed dc-link voltage control method when (a) the first loading is connected and (b) both the first and second loadings are connected.

B. Effectiveness of Proposed DC-Link Voltage Control Method

Withthe implementationof theproposed dc-link voltage control method, Figs. 13 and 15 illustrate the *LC*-HAPF whole simulated and experimental dynamic compensation process for the loading situations, as shown in Fig. 11. Figs. 13(a) and 15(a) show that the simulation and experimental V_{dc_U} and V_{dc_L} level can also be kept at its reference 30 V with start-up self-charging function, this also verifies the effectiveness of the proposed dc-link voltage control method. Compared with Figs. 12(b) and 14(b), Figs. 13(b) and 15(b) clearly illustrate that the *LC*-HAPF can inject different reactive power values, in which the simulated and experimental Q_{cx_f} are varying with respect to different loading situations. As a result, the simulated and experimental Q_{sx_f} can be approximately compensated close to zero no matter when the first loading or both first and second loadings are connected, as shown in Figs. 13(c) and 15(c), in which the simulated and experimental Q_{sx_f} are significantly smaller than that of the dc-link voltage control method, as shown in Fig. 12(c) and 14(c).

Moreover, the proposed dc-link voltage control method can provide satisfactory dynamic response for *LC*-HAPF, as shown in Figs. 16 and 17. In Figs. 16(a) and 17(a), there is a period of time for which the source current waveforms are being settled, this time period is due to the *LC*-HAPF carrying out start-up self-charging process, the dc-link voltage is being charged from 0 V to its reference value $V_{\mathrm{dc}}^*/2 = 30$ V. Therefore, during the start-up process, the larger the dc-link voltage reference, the longer the source current settling time. After the dc-link voltage is controlled as the reference value, the *LC*-HAPF can have a fast dynamic response of less than one cycle after the second loading is connected, as shown in Figs. 16(b) and 17(b).

Tables VI and VII summarize the dynamic reactive power compensation results of the *LC*-HAPF based on the proposed dc-link voltage control method. The three-phase simulated and experimental DPF of source-side can be further improved compared with the results of dc-link voltage control method as reactive current component. The simulated and experimental $\mathrm{THD}_{i_{sx}}$ are within 3.0% and 5.0%. Figs. 13 and 15 and Tables VI and VII verify the effectiveness of the proposed dc-link voltage control method.

In this paper, as the *LC*-HAPF is tested under linear inductive loadings, there does not contain any harmonic components in source current i_{sx} in ideal case. The simulated and experimental $\mathrm{THD}_{i_{sx}}$ values are actually generated by the switching ripples with a fixed hysteresis band. Moreover, the large THD differences between the simulated and experimental results, as shown in Tables IV–VII, are actually due to the difference of component parameters, the resolution of the transducers, the signal conditional circuit error, the digital computation error, and the noise in the experiment.

Compared the simulated and experimental results with the dc-link control method as reactive current component, the proposed method can: 1) also achieve the dc-link voltage control with start-up self-charging function; 2) provide dynamic reactive power compensation; 3) further improve the DPF; and 4) further reduce the rms value of source current i_{sx}. As a result, it is clearly shown that *LC*-HAPF adopting the proposed

TABLE VI
SIMULATION RESULTS BEFORE AND AFTER *LC*-HAPF REACTIVE POWER COMPENSATION WITH PROPOSED DC-LINK VOLTAGE CONTROL METHOD

	Before Compensation			After Compensation			
Different Cases:	Q_{Lx_f} (VAR)	DPF	i_{sx} (A_{rms})	Q_{sx_f} (VAR)	DPF	i_{sx} (A_{rms})	$THD_{i_{sx}}$ (%)
1st inductive loading	121.8	0.786	3.60	-7.1	0.999	2.85	1.5
1st and 2nd inductive loading	176.6	0.833	6.03	16.4	0.998	5.01	2.4

TABLE VII
EXPERIMENTAL RESULTS BEFORE AND AFTER *LC*-HAPF REACTIVE POWER COMPENSATION WITH PROPOSED DC-LINK VOLTAGE CONTROL METHOD

		Before Compensation			After Compensation			
Different Cases:		Q_{Lx_f} (VAR)	DPF	i_{sx} (A_{rms})	Q_{sx_f} (VAR)	DPF	i_{sx} (A_{rms})	$THD_{i_{sx}}$ (%)
1st inductive loading	A	116.0	0.804	3.48	-8.4	0.986	2.89	4.9
	B	114.5	0.815	3.58	-14.9	0.985	3.02	4.7
	C	117.8	0.812	3.58	-4.3	0.987	2.80	4.7
1st and 2nd inductive loading	A	171.4	0.835	5.85	18.7	0.991	5.05	2.9
	B	168.6	0.842	5.91	12.1	0.992	5.16	3.5
	C	172.7	0.841	5.90	24.5	0.989	4.93	3.5

dc-link voltage control method can provide better compensating performances.

VII. CONCLUSION

This paper investigates different dc-link voltage control techniques for a three-phase four-wire center-split *LC*-HAPF during dynamic reactive power compensation. By using conventional dc-link voltage control method as active current component, an extra start-up dc-link precharging control process may be necessary. To achieve the start-up dc-link self-charging function, the dc-link voltage control as reactive current component can be applied; however, it fails to provide dynamic reactive power compensation. Through the proposed dc-link voltage control method:

1) the *LC*-HAPF can achieve start-up dc-link self-charging function;
2) the dc-link voltage of the *LC*-HAPF can be controlled as its reference level;
3) the *LC*-HAPF can provide dynamic reactive power compensation;
4) the adaptive dc-link voltage reference control can be implemented [20].

Finally, simulation and experimental results of the three-phase four-wire center-spilt *LC*-HAPF under dynamic reactive power compensation application are presented to verify all discussions and analysis, and also show the effectiveness of the proposed dc-link voltage control method.

ACKNOWLEDGMENT

The authors would like to thank the Science and Technology Development Fund, Macao SAR Government, and Research Committee of University of Macau for their financial supports.

REFERENCES

[1] J. S. Subjek and J. S. Mcquilkin, “Harmonics-causes, effects, measurements and analysis,” *IEEE Trans. Ind. Electron.*, vol. 26, no. 6, pp. 1034–1042, Apr. 1990.
[2] L. H. S. Duarte and M. F. Alves, “The degradation of power capacitors under the influence of harmonics,” in *Proc. IEEE 10th Int. Conf. Harmonics Quality Power*, Oct. 2002, vol. 1, pp. 334–339.
[3] S. T. Senini and P. J. Wolfs, “Systematic identification and review of hybrid active filter topologies,” in *Proc. IEEE 33rd Annu. Power Electron. Spec. Conf. (PESC)*, 2002, vol. 1, pp. 394–399.
[4] P. Salmerón and S. P. Litrán, “A control strategy for hybrid power filter to compensate four-wires three-phase systems,” *IEEE Trans. Power Electron.*, vol. 25, no. 7, pp. 1923–1931, Jul. 2010.
[5] A. Luo, W. Zhao, X. Deng, Z. J. Shen, and J.-C. Peng, “Dividing frequency control of hybrid active power filter with multi-injection branches using improved $i_p - i_q$ algorithm,” *IEEE Trans. Power Electron.*, vol. 24, no. 10, pp. 2396–2405, Oct. 2009.
[6] A. Luo, Z. K. Shuai, Z. J. Shen, W. J. Zhu, and X. Y. Xu, “Design considerations for maintaining dc-side voltage of hybrid active power filter with injection circuit,” *IEEE Trans. Power Electron.*, vol. 24, no. 1, pp. 75–84, Jan. 2009.
[7] A. Luo, C. Tang, Z. K. Shuai, W. Zhao, F. Rong, and K. Zhou, “A novel three-phase hybrid active power filter with a series resonance circuit tuned at the fundamental frequency,” *IEEE Trans. Ind. Electron.*, vol. 56, no. 7, pp. 2431–2440, Jul. 2009.
[8] H. Fujita and H. Akagi, “A practical approach to harmonic compensation in power systems—Series connection of passive and active filters,” *IEEE Trans. Ind. Appl.*, vol. 27, no. 6, pp. 1020–1025, Nov./Dec. 1991.
[9] F. Z. Peng, H. Akagi, and A. Nabae, “A new approach to harmonic compensation in power systems—A combined system of shunt passive and series active filters,” *IEEE Trans. Ind. Appl.*, vol. 26, no. 6, pp. 983–990, Nov./Dec. 1990.
[10] S. Park, J.-H. Sung, and K. Nam, “A new parallel hybrid filter configuration minimizing active filter size,” in *Proc. IEEE 30th Annu. Power Electron. Spec. Conf. (PESC)*, 1999, vol. 1, pp. 400–405.
[11] D. Rivas, L. Moran, J. W. Dixon, and J. R. Espinoza, “Improving passive filter compensation performance with active techniques,” *IEEE Trans. Ind. Electron.*, vol. 50, no. 1, pp. 161–170, Feb. 2003.
[12] H. Fujita, T. Yamasaki, and H. Akagi, “A hybrid active filter for damping of harmonic resonance in industrial power systems,” *IEEE Trans. Power Electron.*, vol. 15, no. 2, pp. 215–222, Mar. 2000.
[13] H. Akagi, “New trends in active filters for power conditioning,” *IEEE Trans. Ind. Appl.*, vol. 32, no. 6, pp. 1312–1322, Nov./Dec. 1996.
[14] W. Tangtheerajaroonwong, T. Hatada, K. Wada, and H. Akagi, “Design and performance of a transformerless shunt hybrid filter integrated into a three-phase diode rectifier,” *IEEE Trans. Power Electron.*, vol. 22, no. 5, pp. 1882–1889, Sep. 2007.
[15] R. Inzunza and H. Akagi, “A 6.6-kV transformerless shunt hybrid active filter for installation on a power distribution system,” *IEEE Trans. Power Electron.*, vol. 20, no. 4, pp. 893–900, Jul. 2005.
[16] S. Srianthumrong and H. Akagi, “A medium-voltage transformerless ac/dc power conversion system consisting of a diode rectifier and a shunt hybrid filter,” *IEEE Trans. Ind. Appl.*, vol. 39, no. 3, pp. 874–882, May/Jun. 2003.
[17] H. -L. Jou, K. -D. Wu, J.- C. Wu, C. -H. Li, and M. -S. Huang, “Novel power converter topology for three phase four-wire hybrid power filter,” *IET Power Electron.*, vol. 1, pp. 164–173, 2008.
[18] S. Rahmani, A. Hamadi, N. Mendalek, and K. Al-Haddad, “A new control technique for three-phase shunt hybrid power filter,” *IEEE Trans. Ind. Electron.*, vol. 56, no. 8, pp. 2904–2915, Aug. 2009.
[19] S.-U. Tai, M.-C. Wong, M.-C. Dong, and Y.-D. Han, “Some findings on harmonic measurement in Macao,,” in *Proc. 7th Int. Conf. Power Electron. Drive Syst. (PEDS)*, 2007, pp. 405–410.
[20] C.-S. Lam, W.-H. Choi, M.-C. Wong, and Y.-D. Han, “Adaptive dc-link voltage controlled hybrid active power filters for reactive power compensation,” *IEEE Trans. Power Electron.*, vol. 27, no. 4, pp. 1758–1772, Apr. 2012.
[21] X.-X. Cui, C.-S. Lam, and N.-Y. Dai, “Study on dc voltage control of hybrid active power filters,” in *Proc. 6th IEEE Conf. Ind. Electron. Appl. (ICIEA)*, Jun. 2011, pp. 856–861.
[22] C.-S. Lam, M.-C. Wong, and Y.-D. Han, “Voltage swell and overvoltage compensation with unidirectional power flow controlled dynamic voltage restorer,” *IEEE Trans. Power Del.*, vol. 23, no. 4, pp. 2513–2521, Oct. 2008.
[23] B. Singh and V. Verma, “An indirect current control of hybrid power filter for varying loads,” *IEEE Trans. Power Del.*, vol. 21, no. 1, pp. 178–184, Dec. 2005.
[24] M. Aredes, J. Hafner, and K. Heumann, “Three-phase four-wire shunt active filter control strategies,” *IEEE Trans. Power Electron.*, vol. 12, no. 2, pp. 311–318, Mar. 1997.

[25] C.-S. Lam, M.-C. Wong, and Y.-D. Han, "Hysteresis current control of hybrid active power filter," *IET Power Electron.*, to be published.
[26] F. Z. Peng, H. Akagi, and A. Nabae, "A study of active power filters using qudad-series voltage source PWM converters for harmonic compensation," *IEEE Trans. Power Electron.*, vol. 5, no. 1, pp. 9–15, Jan. 1990.
[27] H. Akagi, S. Ogasawara, and K. Hyosung, "The theory of instantaneous power in three-phase four-wire systems: A comprehensive approach," in *Proc. Conf. Rec. IEEE 34th IAS Annu. Meeting*, 1999, vol. 1, pp. 431–439.

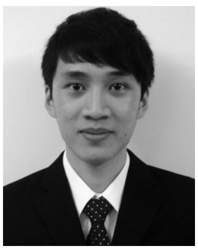

Wai-Hei Choi (S'09) received the B.Sc. degree in electrical and electronics engineering, in 2009, from the University of Macau (UM), Macao, China, where he is currently working toward the M.Sc. degree in a research group of the Power Electronics Laboratory (PE Lab).

His current research interests include power electronics, energy saving, and power quality compensators.

Mr. Choi was the recipient of the Champion Award in the "Schneider Electric Energy Efficiency Cup," Hong Kong, 2010.

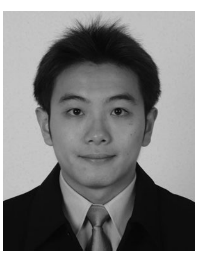

Chi-Seng Lam (S'04) received the B.Sc., M.Sc., and Ph.D. degrees in electrical and electronics engineering from the University of Macau (UM), Macao, China, in 2003, 2006, and 2012, respectively.

From September 2006 to June 2009, he was an E&M Engineer in the Campus Development and Engineering Section at UM. He is currently a Technician of Power Electronics Laboratory (PE Lab) at UM. He has coauthored more than 30 technical journals and conference papers. His current research interests include power electronics, energy saving, power quality, and distribution flexible ac transmission system.

Dr. Lam was the recipient of the Macao Scientific and Technological R&D Award for Postgraduates (Ph.D. level) in 2012. He also received the third Regional Inter-University Postgraduate Electrical and Electronic Engineering Conference Merit Paper Award in 2005.

Man-Chung Wong (SM'06) received the B.Sc. and M.Sc. degrees in electrical and electronics engineering from the University of Macau, Macao, China, in 1993 and 1997, respectively, and the Ph.D. degree from the Tsinghua University, Beijing, China, in 2003.

Sine 2008, he has been an Associate Professor at the University of Macau. His current research interests include flexible ac transmission system and distribution flexible ac transmission system, power quality, custom power, and pulsewidth modulation.

Dr. Wong was the recipient of the Young Scientist Award from the "Instituto Internacional De Macau" in 2000, the Young Scholar Award from the University of Macau in 2001, and second prize of 2003 Tsinghua University Excellent Ph.D. Thesis Award.

Ying-Duo Han (SM'95) was born in Shenyang, Liaoning Province, China, in 1938. He received the B.S. and M.S. degrees from the Department of Electrical Engineering, Tsinghua University, Beijing, China, in 1962 and 1965, respectively, and the Ph.D. degree in electrical engineering from Erlangen-Nuerenberg University, Erlangen, Germany, in 1986.

From 1986 to 1995, he was the Vice-Chairman and Chairman of the Department of Electrical Engineering, Tsinghua University, where he is currently a Professor, and has been the Head of Power Electronics Research Center since 1989. He is also a Visiting Professor at the University of Macau, Macao, China.

Dr. Han was the recipient of five Chinese State-level prizes, and seven first and second ranked Province-level and Ministry-level prizes. He is a Member of the Chinese Academy of Engineering.